Carbon 144 (2019) 351–361

Contents lists available at ScienceDirect

Carbon

journal homepage: www.elsevier.com/locate/carbon

Pilot-scale fabrication and analysis of graphene-nanocomposite fibers

Benjamin A. Weise [a, *], Konstantin G. Wirth [a], Lukas Völkel [a], Markus Morgenstern [b], Gunnar Seide [a]

[a] Aachen-Maastricht Institute for Biobased Materials, Maastricht University, 6167, Geleen, the Netherlands
[b] II. Institute of Physics B, RWTH Aachen University, 52074, Aachen, Germany

ARTICLE INFO

Article history:
Received 20 August 2018
Received in revised form
29 October 2018
Accepted 11 December 2018
Available online 14 December 2018

ABSTRACT

Graphene/polymer composites can be spun into fibers with remarkable mechanical, thermal and electrical properties, but few studies have considered requirements for the pilot-scale production of such fibers using commercially available graphene nanoplatelets (GnP). To address this limitation, we fabricated melt-spun polyamide 6 (PA6) multifilament yarns in which 3% or 5% (w/w) GnP was incorporated into the PA6 matrix by melt compounding during the initial process step. We tested a range of melt-spinning process parameters and analyzed the properties of the resulting fibers in detail. We were able to fabricate yarns containing 24 single filaments at a maximum winding speed of 1800 m/min while applying a draw ratio of 2.5. The electrical conductivity of the as-spun yarns was in the 10 μS/m range, which is suitable for the production of anti-static textiles. Furthermore, the degree of crystallization declined as the GnP content increased, reducing the tenacity of the yarn but improving its elastic modulus, allowing the production of composite textiles. In conclusion, we confirmed that large amounts of graphene can be incorporated into PA6 polymers by melt spinning and that the resulting composite fibers are suitable for multiple downstream applications in the textile industry.

1. Introduction

Graphene is an allotrope of carbon with a unique combination of outstanding mechanical, thermal and electrical properties [1–4]. This makes it suitable for the development of composite materials in applications such as high-performance electronics in the terahertz range [5,6], advanced sensors [7,8], and electrodes in charge-storage devices such as batteries and supercapacitors [9,10].

The properties of several graphene/polymer composites have been investigated. For example, graphene nanoplatelets (GnP) at a concentration 3% (w/w) improved the mechanical and thermal properties and barrier behavior of polypropylene (PP), increasing its elastic modulus from 1.3 to 1.8 GPa [11]. PP composites containing 0.5% (w/v) GnP achieved an electrical conductivity in the mS/m range, which is 10 orders of magnitude higher than pure PP [12]. The incorporation of 2.8% (w/w) exfoliated graphite into PP increased its tensile strength from 28 to 43 MPa, and doubled its elastic modulus to 1.87 GPa [13]. PP composite films containing 3% (w/w) graphene achieved an electrical conductivity of 100 mS/m and a percolation threshold of 1–3% (w/w) [14]. Finally, the elastic modulus of composites containing 0.42% (w/w) GnP was ~74% higher than that of pure PP [15].

The improved properties of graphene/polymer composites are ideal for the fabrication of fibers, which form the basis of yarns used in clothing and technical textiles. Alternatively, graphene can be used as a filler material for high-tenacity yarns or electrically-conductive yarns in smart textiles. Several spinning methods can be used to achieve this goal, including the widely used melt-spinning technique, which is suitable for high-throughput manufacturing [16], and wet spinning, which enables the incorporation of up to 100% filler materials [17].

Several reports describe the successful wet spinning of highly-conductive graphene fibers [18–20]. However, one disadvantage of wet spinning is that graphene oxide rather than graphene is used as the starting material because outstanding electrical properties reflect the highly-oriented carbon structures inside the fibers caused by the nematic phases of graphene oxide. The graphene oxide must be reduced to pure graphene using hazardous materials such as hydrazine. The processing velocities reported thus far are restricted to a few meters per minute.

To overcome these drawbacks, melt spinning has been used to prepare polyethylene terephthalate (PET) monofilaments loaded

* Corresponding author.
E-mail address: benjamin.weise@rwth-aachen.de (B.A. Weise).

https://doi.org/10.1016/j.carbon.2018.12.042

with up to 4% (w/w) graphene, achieving a tensile strength of 640 MPa with an elastic modulus of 16 GPa at 0.31% (w/w) graphene [21]. Monofilaments of graphene and polyamide 6 (PA6) have been prepared by the *in situ* polymerization of ε-caprolactam monomers, initially achieving a tensile strength of 123 MPa and an elastic modulus of 722 MPa [22], later improved to 387 MPa and 3 GPa [23], and finally to 500 MPa and 3 GPa [24]. Similar performance has been reported in other studies, but all the above cases involved a small-scale and low-throughput manufacturing process [25–28].

To fully exploit the properties of graphene-modified polymer fibers, two research projects thus far have addressed pilot-scale manufacturing using commercially available graphene grades and commodity polymers such as PP and PA6. In the first study [29], bicomponent fibers of PP modified with carbon black and up to 10% (w/w) GnP yielded multifilament yarns drawn with a winding velocity of 504 m/min. A total draw ratio of 2.5 was applied but the melt draw ratio was not reported. The electrical conductivity of the as-spun yarns was 3.6 S/m [29]. In the second study, PP multifilament yarns containing 0.2% (w/w) GnP were manufactured at a winding velocity of 2000 m/min using a spinneret die comprising 36 capillaries each 0.25 mm in diameter [30]. Analysis of the distribution of graphene revealed the presence of several micrometer-sized agglomerations of GnP as well as PP crystals promoted by graphene acting as a nucleating agent. The presence of graphene improved the thermal stability of the polymer due to the higher activation energy required for decomposition [30].

We have previously described the properties of graphene-modified polymer fibers produced by melt spinning and wet spinning, including melt-spun PA6 multifilament yarns containing 1% (w/w) GnP with conductivities in the μS range which were suitable for processing into woven fabrics [31]. Here we investigated the influence of commercially available GnP on the properties of melt-spun PA6 multifilament yarns, incorporating 3% or 5% (w/w) GnP into the PA6 matrix by melt compounding followed by melt spinning to develop a viable pilot-scale process for the manufacturing of such composite fibers. Extending our previous work [31], we tested different quantities of GnP in PA6 composite multifilament yarns to determine whether there is a technical limit for graphene incorporation, given that additives often affect the spinnability of polymer melts. We also determined whether graphene-modified fibers are suitable for downstream applications despite the current technical limits.

2. Experimental

2.1. Materials

2.1.1. Raw materials

Commercially available graphene was obtained from Avanzare Innovacion Technologica S.A. (La Rioja, Spain). We used AVANgraphene nanoplatelets (Av-PLAT-2) with a diameter of 2 μm and an average thickness of 10 nm. Polyamide grade B24 N03 in granular form was obtained from BASF AG (Ludwigshafen, Germany). This polymer grade is designed for yarn extrusion and can be processed at temperatures up to 280 °C.

2.1.2. Compound fabrication

Graphene-modified PA6 nanocomposite fibers were prepared from granular master batches containing 10% (w/w) GnP in PA6 fabricated by the melt-mixing of solid-state GnP powder and molten PA6 in a twin-screw compounder. The master batches were fabricated by Geba Kunststoff compounds GmbH, Ennigerloh, Germany. To prepare the 3% and 5% (w/w) GnP/PA6 composites, the 10% (w/w) master batches were diluted with pure solid-state PA6 using an in-house solid-state stirring device.

2.2. Yarn fabrication

A pilot-scale melt-spinning line was used for yarn production (Fourné Maschinenbau GmbH, Alfter-Impekoven, Germany). This comprised a twin-screw extrusion line with three remote controlled temperature zones, a melt line and a spinneret die. A polymer mass throughput of up to 2 kg/h is possible using this system. We produced multifilament yarns consisting of 24 single filaments using a spinneret die with capillary diameters of 0.25 mm and a length-to-diameter ratio of 2.0. After falling through a quench air chamber 175 cm in length, the as-spun yarn was wound using a take-up system manufactured by Comoli Fermo Srl, Paruzzaro, Italy. This comprised a godet duo, followed by two single godets and the winder operating at 190–1800 m/min. Bobbins were wound for 15 min. The extrusion line and winding system are shown in Fig. 1.

2.3. Analysis

The as-spun yarns were analyzed by differential scanning calorimetry (DSC) and thermal gravimetric analysis (TGA) to determine thermal properties, and tensile tests were used for mechanical characterization. Two-point DC resistance measurements were used to determine electrical conductivity. The yarns were visualized by optical and scanning electron microscopy (SEM) and the structure was investigated by wide angle X-ray diffraction (WAXD).

DSC measurements were acquired on a DSC1 gauge (Mettler Toledo AG, Greiffensee, Switzerland) in the temperature range 30–270 °C. The measurements comprised three steps: initial heating at 10 °C/min, immediately followed by cooling at the same rate, and finally heating again at 10 °C/min to isolate structure formation effects induced by fiber spinning. TGA was carried out over the range 35–600 °C at a temperature gradient of 10 °C/min. Furthermore, we used TGA data to investigate the decomposition behavior with respect to the required activation energy, using Equation (1) according to the Horowitz-Metzger method [38]:

$$\ln\ln\left(\frac{1}{1-\alpha}\right) = \frac{E_a \cdot \theta}{R \cdot T_{max}^2} \tag{1}$$

where α is the already decomposed mass fraction at a certain temperature, θ is the difference between the current temperature and the temperature maximum of the decomposition area, and R is the universal gas constant. If the two parts of Equation (1) are plotted against each other, the slope of the line allows the activation energy E_a to be determined.

Two-point DC measurements of Ohmic resistance were taken as previously described with modifications [29] using a Picoammeter Voltage Source Model 6487 E (Keithley Instruments Inc., Cleveland, Ohio, USA). Fiber samples were clamped between two crocodile electrodes at a given distance and the Ohmic resistance was measured at 3 V. By varying the electrode distance, the specific resistance could be determined by linear regression based on the relationship between the Ohmic resistance R_Ω and the specific resistance ρ shown in Equation (2) [32].

$$R_\Omega = \rho \cdot \frac{l}{A} \tag{2}$$

where l is the distance between the electrodes and A the cross-sectional area of the fiber.

Tensile strength was determined according to standard DIN EN 2062 [33] using a Statimat M device (Textechno Herbert Stein GmbH & Co KG, Mönchengladbach, Germany). The fiber was

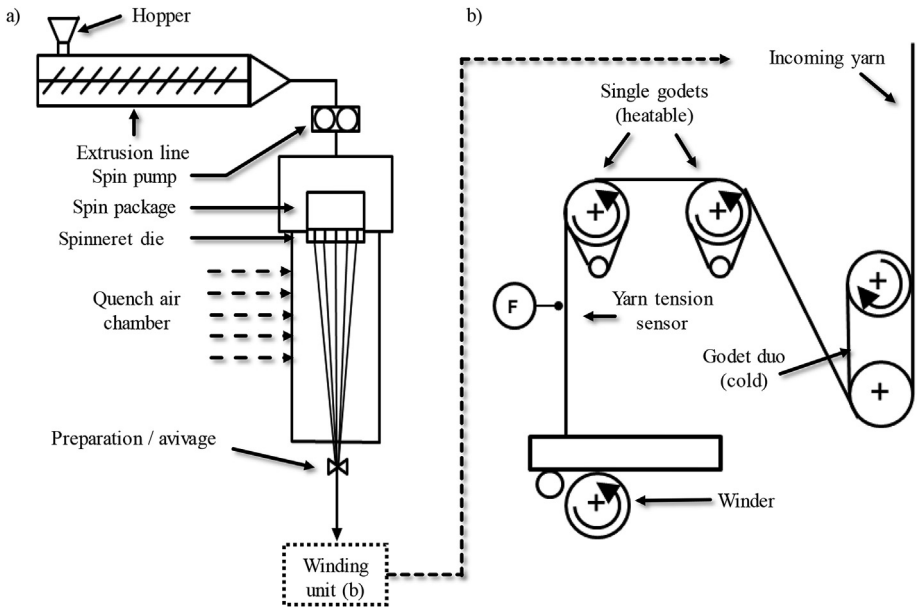

Fig. 1. The pilot-scale extrusion line and winding system used to produce graphene-modified PA6 yarns.

attached to two clamps initially 10 cm apart and a tensile force was applied, increasing the distance between the clamps at a rate of 50 mm/min. The strain was recorded using a dynamo/distance meter connected to computer running software that generates an average force-strain diagram based on 30 measurements per sample. The fiber yarn count was based on three yarn samples of 100 m each, which were weighed according to standard DIN EN 2061 [34].

Optical microscopy to determine fiber quality was carried out using a Leica DM 4000M (Leica Microsystems GmbH, Wetzlar, Germany). Scanning electron microscopy was carried out using a LEO 1450 VP (LEO Electron Microscopy Ltd, Cambridge, UK).

Finally, WAXD was carried out using an IPDS II diffractometer (Stoe GmbH & Co KG, Darmstadt, Germany) with monochromatic X rays of 70.7 pm wavelength (Molybdenum Kα radiation) focused on the samples for 30 min. The intensity diagrams were converted into intensity-over-angle diagrams thus revealing information about the crystallinity of the fiber samples. If the intensity is plotted against the diffraction angle, the diagram consists of an overlap of crystalline peaks and the amorphous background. The area underneath the crystalline peaks and the amorphous background can be fitted using analysis software, and from the resulting peak areas the degree of crystallization can be determined using Equation (3) [41]:

$$X_c = \frac{A_c}{A_c + A_{am}} \tag{3}$$

where A_c is the area below the crystalline peaks and A_{am} is the area of the amorphous background. Detailed information on the measurement procedure (including sample preparation, the analysis setup and data handling methods) are provided in Supporting Information S1.

The influence of the spinning process on the fiber properties was determined by measuring the melt draw ratio (MDR) and the draw ratio, sometimes known as the solid-state draw ratio. The MDR provides information about the solidification of the yarn and the pre-orientation of the polymer. The MDR value was determined by dividing the winding velocity applied on the godet duo by the extrusion velocity as shown in Equation (4).

$$MDR = \frac{v_{godet\ duo}}{v_{extrusion}} . \tag{4}$$

Both the extrusion velocity and the godet duo velocity can be adjusted using the extrusion line control electronics. The draw ratio is related to the stretching of the fiber over the godet rolls, and is calculated by dividing the velocity of the yarn winder by that of the godet duo as shown in Equation (5).

$$Draw\ Ratio = \frac{v_{winder}}{v_{godet\ duo}} . \tag{5}$$

3. Results and discussion

3.1. Spinning process

We prepared yarns using various MDRs and draw ratios at extrusion temperatures of 240–265 °C for 3% (w/w) graphene and 270–285 °C for 5% (w/w) graphene, the latter to overcome the higher viscosity of the polymer melt. Higher temperatures caused the decomposition of the PA6 matrix, as indicated by TGA. The process parameters used for the 3% (w/w) and 5% (w/w) graphene products are summarized in Tables 1 and 2, respectively.

We found that it was possible to spin graphene-modified PA6 multifilament yarns continuously for 15 min without fiber breaks on the godets. For the 5% (w/w) graphene products, the pressure in the spinneret die increased dramatically within 90 min due to GnP clogging the spinning filter, restricting the melt flow in the spinneret die. Examples of the as-spun bobbins are shown in Fig. 2.

3.2. Analysis of yarn properties

3.2.1. Thermal analysis

DSC and TGA measurements of the composite yarns were compared to pure PA6. DSC thermograms of the second melting stage revealed a double peak in the melting curve of pure PA6 caused by the existence of two crystalline phases (Fig. 3).

The first peak at ~210 °C corresponds to the gamma phase and

Table 1
Process parameters for the melt spinning of PA6 containing 3% (w/w) graphene.

Sample name	Winding velocity (m/min)	Draw ratio [1]	Melt draw ratio [1]
V1	800	2.0	22
V2	1200	2.0	33
V3	600	2.0	17
V4	1600	2.0	37
V5	1800	2.25	37
V6	1800	3.0	28

Table 2
Process parameters for the melt spinning of PA6 containing 5% (w/w) graphene.

Sample name	Winding velocity (m/min)	Draw ratio [1]	Melt draw ratio [1]
G_5_1	900	1.5	41
G_5_2	1200	2.0	27
G_5_3	1500	2.5	21
G_5_4	1500	2.5	21
G_5_5	1200	2.0	27
G_5_6	1500	2.5	21

Fig. 2. Examples of graphene-modified PA6 multifilament yarn bobbins. (A colour version of this figure can be viewed online.)

the second to the alpha phase [35]. The addition of graphene reduced the prominence of the gamma peak, with the higher concentration causing greater peak erosion, suggesting that graphene at the concentrations we used causes a shift from the gamma phase towards the alpha phase. Carbon nanomaterials have previously been shown to influence the structure of PA6 in a similar manner [36]. The change in structure was not caused by the spinning process because any effect caused by spinning was eliminated in the first melt, yet we also observed the same phase-shift phenomenon during the second melt. Therefore, the structural reorganization during cooling occurs without polymer pre-orientation.

The addition of graphene also affected the crystallization behavior of the polymer, causing a progressive increase in the crystallization peak (Fig. 4).

The crystallization peak of pure PA6 fibers occurred at 189.5 °C, but this shifted to 194.5 °C for the 3% (w/w) graphene composite and 195.4 °C for the 5% (w/w) graphene composite. This agrees with earlier reports concerning the ability of carbon nanotubes and graphene to act as nucleating agents in polymer materials [37]. The peak width also increased at the higher concentration of graphene, suggesting crystallization occurs over a broader temperature range due to the nucleating activity of the graphene. Compared to the temperature shift between pure PA6 and the 3% (w/w) graphene composite, there was little additional change between the 3% and 5% (w/w) composites, suggesting that the high volume filling of graphene in the polymer resulted in the GnP particles interfering with each other's ability to promote nucleation.

TGA curves of the different fibers are shown in Fig. 5, focusing on the 300–535 °C range for clarity. Both composites decomposed at a slower rate than pure PA6.

For example, ~20% of the pure PA6 decomposed at 400 °C but only 15% of the graphene composites decomposed under the same conditions. The decomposition area can be determined by fitting tangential lines to the decomposition diagram before and after decomposition and marking the crossing points, resulting in the data reported in Table 3.

The activation energies are summarized in Table 4. The addition of 3% and 5% (w/w) graphene increased the activation energy required for the decomposition of the fiber materials by 13.6% and 14.6%, respectively, indicating that graphene increases the thermal stability of PA6. Similar observations have been reported for a polypropylene composite with lower concentrations of graphene [30].

3.2.2. *Tensile analysis*

Tensile analysis was carried out to determine the influence of graphene on the mechanical properties of the melt-spun filaments. Each sample was tested 30 times, allowing the average force-strain to be calculated (Fig. 6). We tested samples with a comparable MDR of ~30 and the highest attainable draw ratio of 2.5.

The tensile strength of the yarns decreased as more graphene was included, reflecting the ability of the GnP particles to act as grain boundaries and perturbing agents. This resulted in higher internal yarn tension at lower strain rates and thus less force was required for fiber rupture (Table 5).

The addition of graphene at levels exceeding 1% (w/w) therefore diminishes the tenacity of the product, as shown by comparing the slopes of the stress-strain curves in the elastic region of pure PA6 and the composites. Based on the definition of the elastic modulus

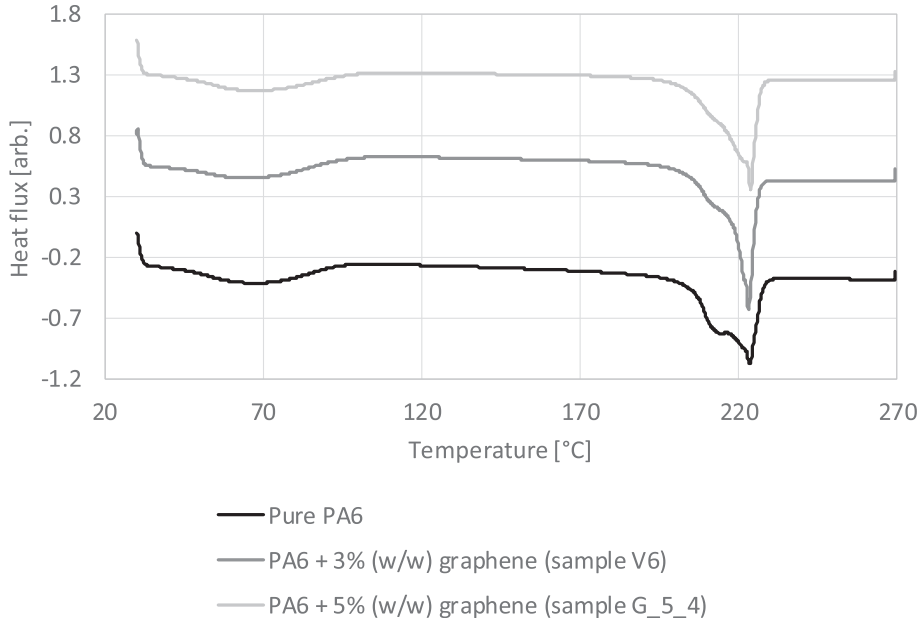

Fig. 3. DSC thermograms of graphene-modified PA6 yarns.

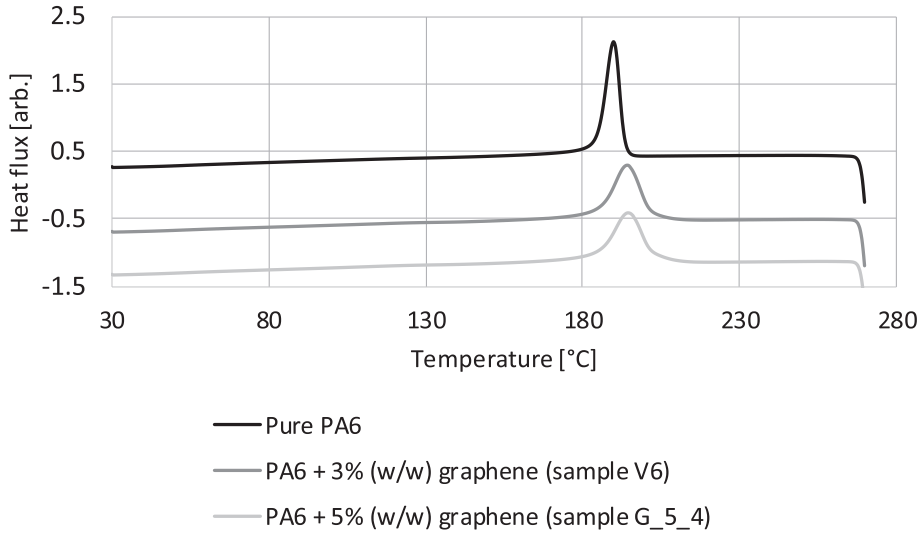

Fig. 4. Crystallization curves of pure PA6 yarns and graphene-modified yarns.

[32], we conclude that GnP increase of the elastic modulus of the yarns, making them suitable for selected composite materials.

Despite the unambiguous tenacity data, the higher elongation at break value for the 5% (w/w) graphene composite defied our expectations and contrasts with the results of many earlier studies. However, a greater elongation at break value was previously reported for PA6 modified with nano-silicates, indicating that the incorporation of filler materials does not automatically reduce elongation at break [43]. We assume that process-induced effects explain our observations, given that the pressure during fiber fabrication increased rapidly during the first hour of spinning. This reflects the fact that graphene particles progressively blocked the spin filters, which would result in the heterogeneous distribution of graphene particles within the fiber. This is supported by our optical analysis data: light microscopy revealed the absence of graphene voids in the fiber whereas electron microscopy provided evidence of heterogeneity in the 5% (w/w) composite, with graphene forming agglomerates on the fiber surface. These results are discussed in more detail below (Figs. 7–9).

3.2.3. Electrical conductivity

The electrical conductivity of the yarns was measured by two-point DC resistance analysis applying a voltage of 3 V, and yarns with different draw ratios were measured to determine whether the spinning process had any effect on the electrical properties. The electrical conductivity of pure PA6 is 10^{-12} S/m [39]. The presence of 3% (w/w) graphene increased the conductivity of the yarn by six orders of magnitude. Furthermore, we observed an inverse relationship between the conductivity and the draw ratio (Table 6). This indicates that the number of overlapping graphene sheets inside the fiber declines when the fiber is drawn. In agreement with the percolation model of electrical conductivity, this suggests there are

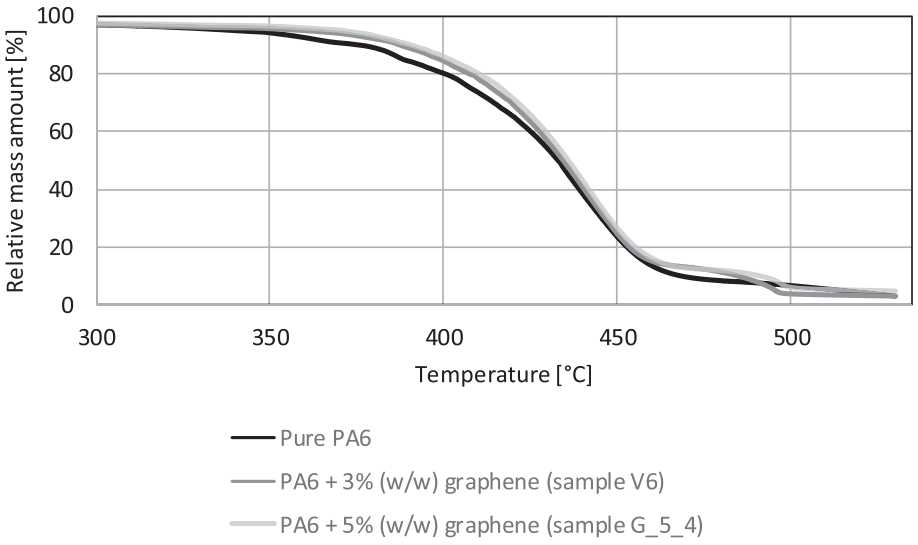

Fig. 5. TGA curves of graphene-modified PA6.

Table 3
Decomposition areas of pure PA6 and graphene-modified PA6.

Yarn sample	Decomposition area [°C]
Pure PA6	406–461
PA6 + 3% (w/w) graphene (sample V6)	409–463
PA6 + 5% (w/w) graphene (sample G_5_4)	412–467

Table 4
Activation energies of pure PA6 and graphene-modified PA6.

Yarn sample	Activation energy [kJ/mol]
Pure PA6	66.28 ± 0.24
PA6 + 3% (w/w) graphene (sample V6)	74.60 ± 0.77
PA6 + 5% (w/w) graphene (sample G_5_4)	75.93 ± 3.50

fewer conductive paths in the fiber and thus a lower conductivity [40]. The presence of 5% (w/w) graphene did not result in a further significant increase in conductivity compared with the 3% (w/w) graphene composite (Table 7). The Ohmic resistances of the fibers with the highest electrical conductivities are shown in Table 8.

Overall, the electrical conductivity values were relatively low compared to earlier reports using graphene and carbon nanotubes [29], possibly reflecting the quality of the GnP. Interestingly, the conductivity increased at higher draw ratios in the 5% (w/w) graphene composite, in contrast to the effect observed in the 3% (w/w) composite and also in disagreement with earlier studies [29,37]. A potential explanation of this behavior is discussed below. Furthermore, the diameter of the 5% (w/w) graphene fiber was more homogenous at higher draw ratios compared to the 3% (w/w)

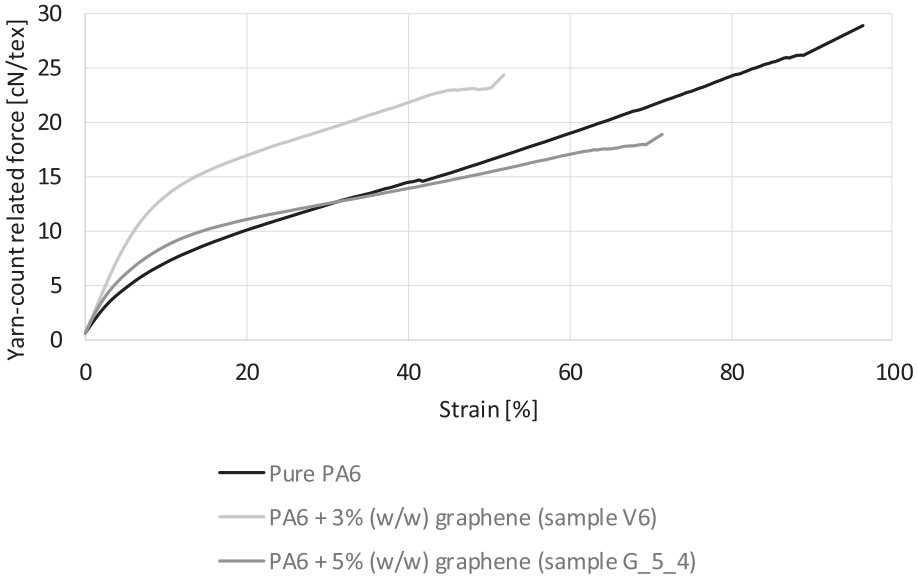

Fig. 6. Stress-strain curves of pure PA6 and graphene-modified PA6 yarns.

Table 5
Tenacities and yarn counts of pure PA6 and graphene-modified PA6.

Yarn sample	Yarn-count related tenacity [cN/tex]	Elongation at break [%]	Yarn count [dtex]
Pure PA6	28.70 ± 1.53	97.27 ± 7.84	258.12 ± 0.02
PA6 + 3% (w/w) graphene (sample V6)	24.40 ± 0.85	51.46 ± 5.23	141.83 ± 0.62
PA6 + 5% (w/w) graphene (sample G_5_4)	18.97 ± 0.92	71.65 ± 5.80	213.51 ± 1.00

The yarn count unit is the decitex (dtex) whereby 1 dtex = 1 g mass per 10,000 m yarn length.

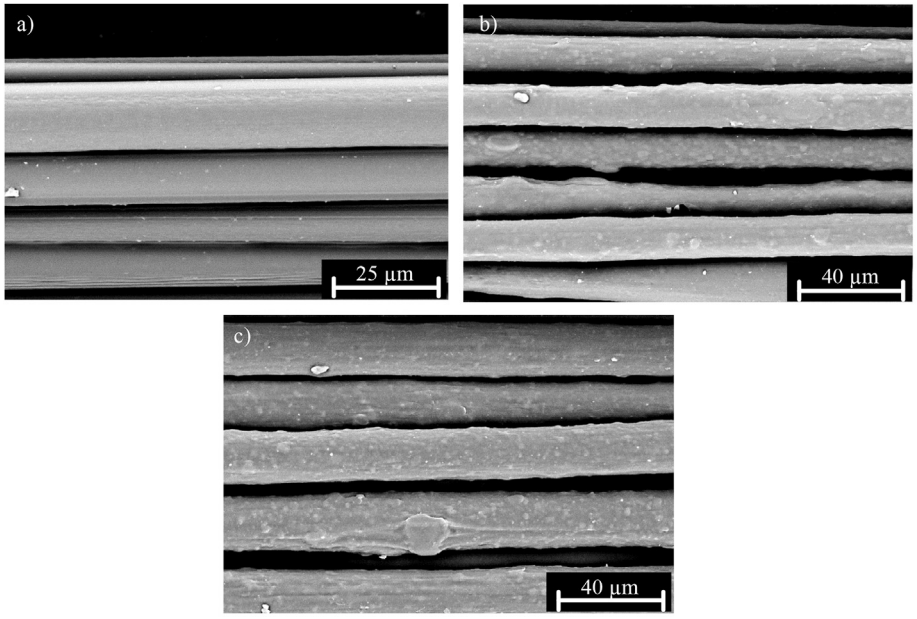

Fig. 7. Scanning electron microscopy images of pure PA6 yarns (a) and PA6 containing 3% (b) and 5% (w/w) graphene (c).

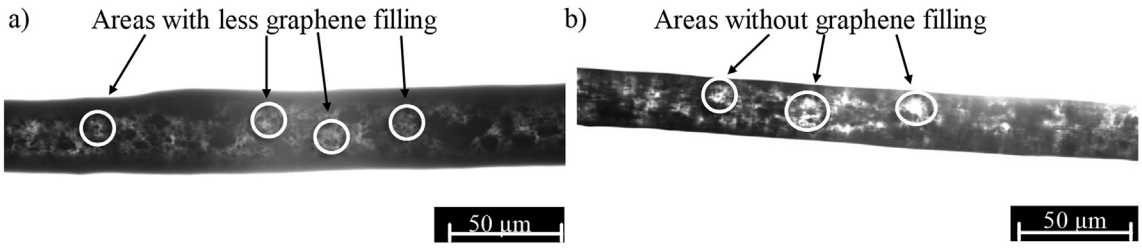

Fig. 8. Optical microscopy image of a single filament modified with 3% (w/w) graphene and a draw ratio of 2 (a) and 3 (b).

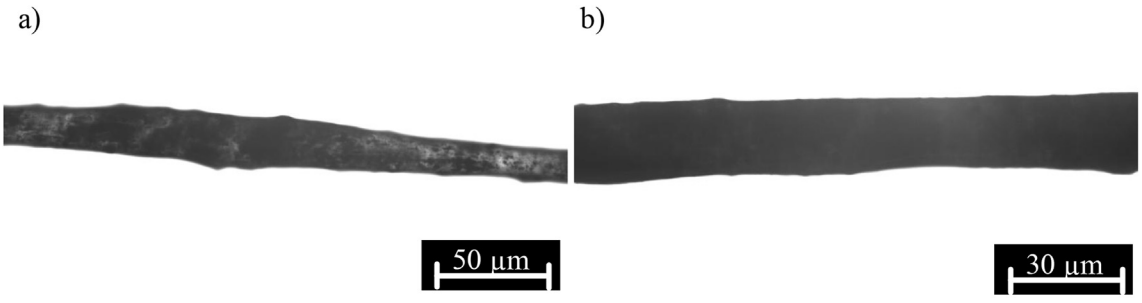

Fig. 9. Optical microscopy image of a single filament modified with 5% (w/w) graphene and a draw ratio of 1.5 (a) and 2.5 (b).

graphene fiber (see microscopy images below), avoiding the restriction of electron transport caused by intermittent fiber narrowing (necking) observed in other conducting nanostructures [42]. Another potential explanation for the conductivity behavior in the presence of 5%(w/w) graphene reflects the mechanism of electrical conductivity inside the graphene-modified filament, as shown in the model provided in Supporting Information S2. Given the higher quantity of graphene filler in the 5%(w/w) graphene

Table 6
Electrical conductivities of PA6 multifilament yarns containing 3% (w/w) graphene.

Yarn sample with draw ratio	Electrical conductivity [μS/m]
V2 (DR = 2)	12.13 ± 0.44
V4 (DR = 2)	7.23 ± 0.03
V5 (DR = 2.25)	8.03 ± 0.03
V6 (DR = 3)	6.40 ± 1.25
PA6 reference	10^{-6}

Table 7
Electrical conductivities of PA6 multifilament yarns containing 5% (w/w) graphene.

Yarn sample with draw ratio	Electrical conductivity [μS/m]
G_5_1 (DR = 1.5)	8.26 ± 0.04
G_5_2 (DR = 2)	10.71 ± 2.14
G_5_4 (DR = 2.5)	14.56 ± 0.59
PA6 reference	10^{-6}

fibers, the probability of tunnel currents within the filament increases which may compensate for the loss of conductivity caused by fiber drawing. In order to achieve percolation, the mass fraction of the graphene platelets must increase substantially in comparison to the as-spun yarns, which is not possible in current pilot-scale spinning processes due to the rapid clogging of the spin filter systems.

Furthermore, according to the standard percolation model [46], the conductivity of a composite material is almost identical to that of the matrix material if there is a low concentration of filler, followed by a sharp increase in conductivity within a very small window of filler concentration. In the case of graphene and graphite platelets, even low concentrations of filler result in a continuous increase in electrical conductivity over several orders of magnitude [44,45], in contrast to the results seen with carbon nanotubes [37] and thus highlighting the need for more detailed analysis of conductivity mechanisms in composites containing two-dimensional nanomaterials.

Although the conductivities we observed (in the μS/m range) are far below the maxima reported in earlier studies [15,18,29], the as-spun filaments are suitable for anti-static textile applications because the filaments show dissipative properties. Furthermore, although a higher graphene content would improve the electrical conductivity of the fibers, making them suitable for high-performance applications such as smart textiles, the presence of more filler would also make the fibers stiffer, thus making them less suitable for products like knitted fabrics in which high flexural strengths are required. Accordingly, lower conductivities do not necessarily restrict the usability of the fibers, because fibers with different conductivities are required for different applications.

3.2.4. Optical analysis

The comparison of pure PA6 fibers with the 3% and 5% (w/w) graphene composites by SEM revealed a significant difference in surface features and graphene distribution (Fig. 7).

The pure PA6 fibers featured a smooth surface and a homogenous, constant diameter. The incorporation of 3% (w/w) graphene resulted in heterogeneities caused by agglomerations of graphene. Several 'dents' formed by graphene flakes were visible, indicating that the graphene agglomerations were similar in size to the filament diameter (10 μm). These agglomerations were even larger and more abundant in the 5% (w/w) graphene composite. Optical transmission microscopy was carried out to determine the distribution of graphene in the fiber and the potential effects of the drawing process. Fig. 8 shows 3% (w/w) graphene fibers with draw ratios of 2 and 3.

The heterogeneous graphene distribution was apparent at the lower draw ratio as shown by the appearance of bright scales representing areas with less graphene filling. When the draw ratio was increased to 3, white spots appeared representing areas with no graphene filling at all. Such voids would inhibit the passage of electrons through the fiber, explaining the lower conductivity at higher draw ratios. Fig. 9 shows 5% (w/w) graphene fibers with draw ratios of 1.5 and 2.5. The distribution of graphene in these samples is much more homogeneous, with fewer gray patches indicating areas with less graphene filling, particularly in the sample with the higher draw ratio. The electrical conductivities of these fibers are therefore higher despite the higher draw ratio.

3.2.5. Structural analysis

Structural analysis by WAXD revealed that the intensity of the reflection patterns declined progressively as the graphene content increased, and the signal was almost obliterated in the 5% (w/w) graphene composite (Fig. 10).

The WAXD patterns were converted into intensity-over-angle diagrams (Fig. 11).

The degree of crystallization was determined for fibers spun with a draw ratio of 2.5 (Table 9).

In the 5% (w/w) graphene composites, the degree of crystallization was lower than pure PA6 and the 3% (w/w) composite, which appears to contradict the assumptions made based on our thermal analysis experiments. However, the ability of graphene to act as a nucleating agent does not necessarily infer that the degree of crystallization increases. Similar observations, i.e. that graphene acts as a nucleating agent but does not increase the crystallinity of the composite, have been reported for graphene-modified polypropylene [12]. We assume that the graphene platelets promote crystallization (as shown by the higher crystallization temperatures) but simultaneously impair crystallization due to the high content of graphene, which results in mutual interference between adjacent crystallites. We can exclude the influence of the spinning process and/or the applied temperature because all yarns were spun with a draw ratio of 2.5 to achieve comparable samples, so the influence of the solid-state drawing process would be the same for each fiber sample. Although there were differences in the MDR between samples, PA6 crystallizes more slowly than polypropylene and polyethylene and the nano-composite fibers therefore adopt an almost completely amorphous state as they are wound on the first godet duo. Therefore, further drawing on the godets is responsible for yarn properties such as tenacity. Even if pre-orientation had affected the tenacity of the yarn, this would have been eliminated because the yarns were heated to 80 °C on the godet during solid-state drawing. This is above the glass transition temperature of PA6

Table 8
Ohmic resistances of PA6 multifilament yarns containing 3% and 5% (w/w) graphene.

Yarn sample	Ohmic resistance [GΩ]		
	Distance: 2 cm	Distance: 4 cm	Distance: 6 cm
3% w/w graphene (sample V2)	172.2 ± 50.4	245.3 ± 38.8	402.0 ± 91.8
5% w/w graphene (sample G_5_4)	58.3 ± 21.1	81.5 ± 11.1	105.2 ± 19.5

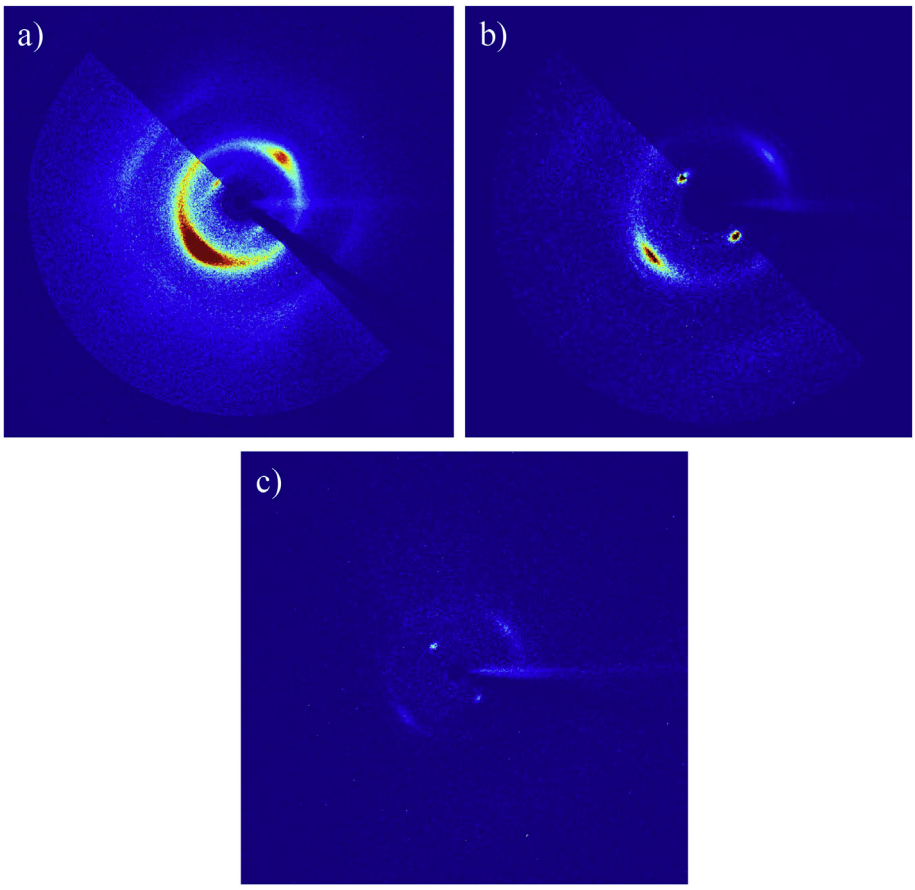

Fig. 10. WAXD image of pure PA6 (a) and PA6 containing 3% (b) and 5% (w/w) graphene (c). (A colour version of this figure can be viewed online.)

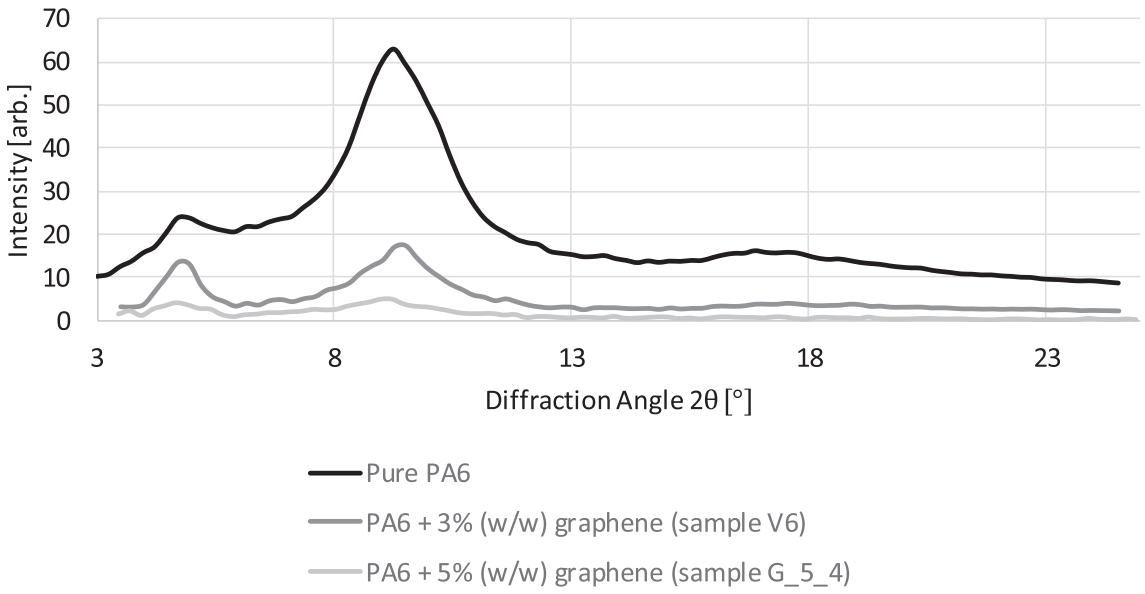

Fig. 11. Intensity-over-angle diagrams for pure PA6 and PA6 containing 3% and 5% (w/w) graphene.

where the amorphous component is therefore movable, enabling the polymer chains to be re-oriented during the solid-state drawing process. Furthermore, the influence of the spinning parameters on the thermal properties and phase transitions of the yarn samples can be excluded based on the second heating curve of the DSC measurements. The most important effects of graphene on the behavior of PA6 composites can therefore be summarized as follows:

Table 9
Degree of crystallization values for pure PA6 and composites containing 3% and 5% (w/w) graphene.

Yarn sample	Degree of crystallization (%)
Pure PA6	25.1 ± 3.0
PA6 + 3% (w/w) graphene (sample V6)	26.9 ± 2.6
PA6 + 5% (w/w) graphene (sample G_5_4)	12.4 ± 4.5

1. The incorporation of GnP increases the electrical conductivity of PA6 by several orders of magnitude, up to 10 μS/m
2. Due to its high mass concentration, GnP impairs the development of highly crystalline fibers even though carbon nanomaterials act as nucleating agents in polymers, as highlighted by the observed increase in the crystallization temperature
3. GnP promotes transitions from the polyamide's gamma phase to the alpha phase
4. The tenacity declines as the GnP content increases, whereas the elongation at break recovers slightly as the content of GnP increases from 3% to 5% (w/w); the tenacities are sufficient for further processing of the as-spun yarns, e.g. by weaving.

4. Conclusion and outlook

We have developed a pilot-scale melt-spinning process for the fabrication of graphene-modified multifilament yarns. We achieved graphene mass loadings of up to 5% (w/w) and were able to fabricate multifilament yarns with winding velocities of 1800 m/min, which is the highest reported yield at these mass loadings. The as-spun yarns were characterized by thermal, mechanical, electrical and structural analysis. Thermal analysis confirmed that graphene acts as nucleating agent and increases the activation energy for PA6 decomposition. This observation could be used for the development of textile materials with enhanced flame retardancy. Although the tenacity of the yarns declined with increasing graphene loads, the elastic modulus increased as the slope of the stress-strain curves increased in the elastic regime. We observed electrical conductivities in the range of 10^{-6} S/m, suggesting the as-spun yarns could be used for the development of anti-static textiles. Finally, the influence of GnP on the structural formation of the yarns was investigated by microscopy and WAXD. In future experiments, the spinning process should be improved to fabricate yarn materials with a better electrical and mechanical performance. Our pilot-sale process is a step forward in the application of graphene in the textile industry. The yarns prepared in this study should be further processed into structures such as woven and knitted fabrics in order to investigate the multi-functionality of graphene-based textiles. As well as anti-static and flame-retardant textiles, graphene-modified materials could be developed as battery electrodes, supercapacitors or shielding materials for protection against electromagnetic radiation.

Funding statement

Prof. Markus Morgenstern acknowledges support from the European Union Horizon 2020 Programme under Grant Agreement no. 785219 (Graphene Flagship Core 2). This work is furthermore part of the research programme FLAG-ERA II with project number 680.NFLAG.2, which is partly financed by the Netherlands Organisation for Scientific Research (NWO).

Acknowledgements

We acknowledge the Institute für Textiltechnik (ITA) of RWTH Aachen University for support during the spinning trials and the analysis of the as-spun yarns. We also thank the Institute of Crystallography (IFK) for help with the WAXD analysis and Dr. Thomas Vad from ITA for fruitful discussions on the obtained measurement data.

Appendix A. Supplementary data

Supplementary data to this article can be found online at https://doi.org/10.1016/j.carbon.2018.12.042.

References

[1] A.C. Ferrari, F. Bonaccorso, V. Fal'ko, K.S. Novoselov, S. Roche, P. Boggild, et al., Science and technology roadmap for graphene, related two-dimensional crystals, and hybrid systems, Nanoscale 7 (2015) 4598–4810.
[2] K.I. Bolotin, K.J. Sikes, Z. Jiang, M. Klima, G. Fudenberg, J. Hone, et al., Ultrahigh electron mobility in suspended graphene, Solid State Commun. 146 (2008) 351–355.
[3] J.C. Charlier, P.C. Eklund, J. Zhu, A.C. Ferrari, Electron and phonon properties of graphene: their relationship with carbon nanotubes, in: A. Jorio, G. Dresselhaus, M.S. Dresselhaus (Eds.), Topics in Applied Physics 111, 2008, pp. 673–709.
[4] W. Wei, Q. Xiaogang, Extraordinary physical properties of functionalized graphene, Small 8 (2012) 2138–2151.
[5] I. Llatser, C. Kremers, A. Cabellos-Aparicio, J.M. Jornet, E. Alarcón, D.N. Chigrin, Graphene-based nano-patch antenna for terahertz radiation, Photonics Nanostruct.: Fundam. Appl 10 (4) (2012) 353–358.
[6] J. Tong, M. Muthee, S.-Y. Chen, S.K. Yngvesson, J. Yan, Antenna enhanced graphene THz emitter and detector, Nano Lett. 15 (8) (2015) 5295–5301.
[7] C.I.L. Justino, A.R. Gomes, A.C. Freitas, A.C. Duarte, T.A.P. Rocha-Santos, Graphene based sensors and biosensors, Trends Anal. Chem. 91 (2017) 53–66.
[8] J. Park, J. Kim, K. Kim, S.-Y. Kim, W.H. Cheong, K. Park, et al., Wearable, wiresless gas sensors using highly stretchable and transparent structures of nanowires and graphene, Nanoscale 8 (10) (2016) 10591–10597.
[9] Y. Xie, Y. Liu, Y.-H. Tsang, S.P. Lau, H. Huang, Y. Chai, Stretchable all-solid state supercapacitor with wavy shaped polyaniline/graphene electrode, J. Mater. Chem. A 2 (24) (2014) 9142–9149.
[10] H. Kim, K.-Y. Park, J. Hong, K. Kang, All-graphene-battery: bridging the gap between supercapacitors and lithium ion batteries, Sci. Rep. 4 (2014) 5278–5285.
[11] K. Kalaitzidou, H. Fukushima, L.T. Drzal, A new compounding method for exfoliated graphite-polypropylene nanocomposites with enhanced flexural properties and lower percolation threshold, Compos. Sci. Technol. 67 (2007) 2045–2051.
[12] K. Kalaitzidou, H. Fukushima, P. Askeland, L.T. Drzal, The nucleating effect of exfoliated graphite nanoplatelets and their influence on the crystal structure and electrical conductivity of polypropylene nanocomposites, J. Mater. Sci. 43 (2008) 2895–2907.
[13] K. Wakabayashi, C. Pierre, D.A. Dikin, R.S. Ruoff, T. Ramanathan, L.C. Brinson, et al., Polymer-graphite nanocomposites: effective dispersion and major property enhancement via solid-state shear pulverization, Macromolecules 41 (2008) 1905–1908.
[14] J.-E. An, G.W. Jeon, Y.G. Jeong, Preparation and properties of polypropylene nanocomposites reinforced with exfoliated graphene, Fibers Polym. 13 (4) (2012) 507–514.
[15] P. Song, Z. Cao, Y. Cai, L. Zhao, Z. Fang, S. Fu, Fabrication of exfoliated graphene-based polypropylene nanocomposites with enhanced mechanical and thermal properties, Polymer 52 (18) (2011) 4001–4010.
[16] F. Fourne, Synthetic Fibers: Machines and Equipment Manufacture, Properties, first ed., Carl Hanser Verlag, Munich, Germany, 1999.
[17] N. Behaptu, C.C. Young, D.E. Tsentalovich, O. Kleinermann, X. Wang, A.W.K. Ma, et al., Strong, light, multifunctional fibers of carbon nanotubes with ultrahigh conductivity, Science 339 (6116) (2013) 182–186.
[18] Z. Xu, C. Gao, Graphene fiber: a new trend in carbon fibers, Mater. Today 18 (9) (2015) 480–492.
[19] Y. Zhang, Y. Li, P. Ming, Q. Zhang, T. Liu, L. Jiang, Q. Cheng, Ultrastrong bioinspired graphene-based fibers via synergistic toughening, Adv. Mater. 28 (14) (2016) 2834–2839.
[20] X. Zhao, Z. Xu, B. Zheng, C. Gao, Macroscopic assembled, ultrastrong and H2SO4-resistant fibres of polymer-grafted graphene oxide, Sci. Rep. 3 (2013) 3164–3170.
[21] U. Khan, Y. Karen, A. O'Neill, J.N. Coleman, High strength composite fibres from polyester filled with nanotubes and graphene, J. Mater. Chem. 22 (25) (2012) 12907–12911.
[22] Z. Xu, C. Gao, In situ polymerization approach to graphene-reinforced nylon-6 composites, Macromolecules 43 (2010) 6716–6723.
[23] H. Liu, L. Hou, W. Peng, W. Zhang, X. Zhang, Fabrication and characterization of polyamide 6-functionalized graphene composite fiber, J. Mater. Sci. 47 (23) (2012) 8052–8060.
[24] H.-H. Liu, W.-W. Peng, L.-C. Hou, X.-C. Wang, X.-X. Zhang, The production of a melt-spun functionalized graphene/poly(ε-caprolactam) nanocomposite fiber,

Compos. Sci. Technol. 81 (2013) 61–68.
[25] W. Hou, B. Tang, L. Lu, J. Sun, J. Wang, C. Qin, L. Dai, Preparation and physic-mechanical properties of amine-functionalized graphene/polyamide 6 nanocomposite fiber as a high performance material, RSC Adv. 4 (10) (2014) 4848–4855.
[26] S.H. Hwang, B.J. Kim, J.B. Baek, H.S. Shin, I.-J. Bae, S.Y. Lee, Y.B. Park, Effects of process parameters and surface treatments of graphene nanoplatelets on the crystallinity and thermomechanical properties of polyamide 6 composite fibers, Compos. B Eng. 100 (1) (2016) 220–227.
[27] H.-H. Liu, W.-W. Peng, L.-C. Hou, X.-C. Wang, X.-X. Zhang, The production of a melt-spun functionalized graphene/poly(ε-caprolactam) nanocomposite fiber, Compos. Sci. Technol. 81 (1) (2013) 61–68.
[28] L. Zhou, H. Liu, X. Zhang, Graphene and carbon nanotubes for the synergistic reinforcement of polyamide 6 fibers, J. Mater. Sci. 50 (7) (2015) 2797–2805.
[29] E. Nilsson, H. Oxfall, W. Wandelt, R. Rychwalski, B. Hagström, Melt spinning of conductive textile fibers with hybridized graphite nanoplatelets and carbon black filler, J. Appl. Polym. Sci. 130 (4) (2013) 2579–2587.
[30] B. Kalantari, M.R.M. Mojtahedi, F. Sharif, R.S. Rahbar, Effect of graphene nanoplatelets presence on the morphology, structure and thermal properties of polypropylene in fiber melt-spinning process, Polym. Compos. 36 (2) (2015) 367–375.
[31] B. Weise, L. Völkel, G. Köppe, S. Schriever, J. Mroszczok, J. Köhler, et al., Melt- and wet-spinning of graphene-polymer nano-composite fibres of multifunctional textile applications, Mater. Today: Proceedings 4 (2017) S135–S145.
[32] C. Kittel, Introduction to Solid State Physics, eighth ed., Wiley, Hoboken NJ, 2004.
[33] DIN EN ISO 2062, Textiles – Yarn from Packages – Determination of Single-end Breaking Force and Elongation at Break Using Constant Rate of Extension, Beuth Verlag, Berlin, Germany, 1995.
[34] DIN EN ISO 2060, Textiles – Yarn from Packages – Determination of linear density (mass per unit length) by the skein method, Beuth Verlag, Berlin, Germany, 1995.
[35] W. Steinmann, S. Walter, M. Beckers, G. Seide, T. Gries, Thermal analysis of phase transitions and crystallization in polymeric fibers, in: A.A. Elkordy (Ed.), Applications of Calorimetry in a Wide Context: Differential Scanning Calorimetry, Isothermal Titration Calorimetry and Minicalorimetry, InTechEurope, Rieka, Croatia, 2013, pp. 277–306.
[36] T. Vad, J. Wulfhorst, T.T. Pan, W. Steinmann, S. Dabringhaus, M. Beckers, et al., Orientation of well-dispersed multiwalled carbon nanotubes in melt-spun polymer fibers and its impact on the formation of the semicrystalline polymer structure: a combined wide-angle X-ray scattering and electron tomography study, Macromolecules 46 (14) (2013) 5604–5613.
[37] W. Steinmann, T. Vad, B. Weise, J. Wulfhorst, G. Seide, T. Gries, et al., Extrusion of CNT-modified polymer with low viscosity – influence of crystallization and CNT orientation on the electrical properties, Polym. Polym. Compos. 21 (8) (2013) 473–482.
[38] H.H. Horowitz, G. Metzger, A new analysis of thermogravimetric traces, Anal. Chem. 35 (10) (1963) 1464–1468.
[39] T.A. Osswald, E. Baur, S. Brinkmann, K. Oberbach, E. Schmachtenberg, International Plastics Handbook, The Resource for Plastics Engineers, fourth ed., Carl Hanser Verlag, Munich, Germany, 2006.
[40] A. Bunde, W. Dieterich, Percolation in composites, Journ Electrocer 5 (2) (2000) 81–92.
[41] D.R. Salem, Structure Formation in Polymeric Fibers, first ed., Carl Hanser Verlag, Munich, Germany, 2001.
[42] M.G. Pala, S. Baltazar, P. Liu, H. Sellier, B. Hackens, F. Martins, et al., Transport inefficiency in branched-out mesoscopic networks: an analog of the Braess paradox, Phys. Rev. Lett. 108 (2012) 076802.
[43] W. Steinmann, S. Walter, T. Gries, G. Seide, G. Roth, Modification of the mechanical properties of polyamide 6 multifilaments in high-speed melt spinning with nano cilicates, Textil. Res. J. 82 (18) (2012) 1846–1858.
[44] H.-B. Zhang, W.-G. Zheng, Q. Yan, Y. Yang, J.-W. Wang, Z.-H. Liu, et al., Electrically conductive polyethylene terephthalate/graphene nanocomposites prepared by melt compounding, Polymer 51 (5) (2010) 1191–1196.
[45] J. Du, L. Zhao, Y. Zeng, L. Zhang, F. Li, P. Liu, et al., Comparison of electrical properties between multi-walled carbon nanotube and graphene nanosheet/high density polyethylene composites with a segregated network structure, Carbon 49 (4) (2011) 1094–1100.
[46] J.P. Clerc, G. Giraud, J.M. Laugier, J.M. Luck, The electrical conductivity of binary disordered systems, percolation clusters, fractals and related models, Adv. Phys. 39 (1990) 191–309.